JOURNAL OF MATERIALS SCIENCE 21 (1986) 457–468

The effects of N_2^+ and B^+ ion implantation on the hardness behaviour and near-surface structure of SiC

S. G. ROBERTS*, T. F. PAGE
Department of Metallurgy and Materials Science, University of Cambridge, Pembroke Street, Cambridge, UK

The effects of ion implantation on the near-surface deformation behaviour and structure of both single crystal (6H) silicon carbide and a reaction-bonded SiC composite (REFEL) have been studied using 80 keV N_2^+ and 40 keV B^+ ions in the dose range 1 to 1 × 10^{17} ions cm^{-2}. The ion species were chosen to have different effects on the polytype stability of SiC but produce similar distributions of damage. Subsequent room temperature, load-variant, indentation hardness tests showed that N_2^+ implantations produced a marked near-surface softening above a critical dose of ~4 × 10^{17} ions cm^{-2}. The effect, which appeared specific to N_2^+ implantation, is possibly attributable to the rapid thickening of the surface amorphized damage layer by nitrogen gas bubble formation. Implantation with both species suppressed the break-out of the lateral cracks produced by indentation fracture and this is presumed due to the production of a compressive surface stress. Scratch tests established that even the lowest doses of both species suppressed chipping to the extent that scratch tracks appeared plastically deformed only. Subsequent TEM examination showed that the microcrystalline or amorphous material produced by implantation with either species had transformed during deformation to the low-temperature-stable cubic (3C) polytype despite the differing expected influences of boron and nitrogen on polytype stability.

1. Introduction

Ion implantation is a surface treatment technique whereby energetic ions may be used to significantly modify the structural, chemical and mechanical properties of the near-surface region of materials to depths governed by the ion range and typically being less than ~5 μm (e.g. ~0.2 μm for 100 kV N_2^+ into SiC). Many of the detailed effects arising from the radiation damage, amorphization and surface stresses so induced have been recently described (e.g. [1]). The investigations reported here formed part of an earlier broader study aimed at investigating the basis of the observations of Dearnaley [2] that nitrogen implantation to doses > ~ 4 × 10^{17} cm^{-2} could significantly improve the wear lifetimes of WC–Co composites (and other materials). Since at the time the work was performed there had been otherwise very few investigations of the effects of ion implantation on the mechanical properties of non-metals, the study [3] investigated the effects of ion implantation (mainly N_2^+) on several materials covering a wide range of bond types and plastic/brittle character (e.g. silicon, silicon carbide, alumina WC–Co, cobalt, LiF, metallic and inorganic glasses). Some initial results from the silicon and the silicon carbide materials have already been reported [4], where it was first established that high dose N_2^+-implantation (> ~ 10^{17} ions cm^{-2}) into both materials produced a marked surface softening (as measured by low-load indentation tests) together with suppression of the lateral type of indentation fracture. The present paper gives the results of extended investigations of the effects of boron and nitrogen implantation on the structure and mechanical properties of silicon carbide. While nitrogen was the principal ion species used, boron implantations were also performed. These two ions are very similar in mass (and thus damage characteristics), but have different doping effects on SiC (nitrogen n-type, boron p-type) and are believed to have different effects on polytype stability (e.g. [5]).

Near-surface plastic flow was investigated by microhardness testing. Specifically, study of the variation of measured hardness with size of indentations allowed some conclusions to be drawn about the plastic properties of the thin, near-surface, implanted layer. Fracture patterns around indentations and scratch tracks were examined by light microscopy and scanning electron microscopy (SEM). The structure of the material beneath scratch tracks in both implanted and unimplanted material was examined by transmission electron microscopy (TEM), with particular reference to possible phase transitions induced by the different implant species.

2. Characteristics of the implanted layer

The composition and microstructure of the implanted surface layer vary throughout its depth (e.g. [6]).

*Present address: Department of Metallurgy and Science of Materials, University of Oxford, Parks Road, Oxford, UK.

0022–2461/86 $03.00 + .12 © 1986 Chapman and Hall Ltd.

However, for the purposes of interpreting the results presented here, it is convenient to treat the layer as a simple entity having properties different from those of the bulk material. In any case, the methods used, apart from the TEM techniques, are insufficiently sensitive to detect any variation in properties with depth in the implanted layer. There are four main ways in which the layer differs from the bulk.

1. The accumulation of displacement damage often causes the implanted layer to be non-crystalline at high doses. This is particularly the case for covalently bonded materials implanted at low temperatures, as here. The amorphization of silicon by ion implantation has been intensively studied [6–8]. Typically, amorphization doses are 10^{14} to 10^{15} ion cm^{-2}, though a critical energy deposition density is a more fundamental criterion (e.g. [6]). Silicon carbide is predominantly covalent with a threshold displacement energy (50 to 100 eV [9, 10]) approximately five times greater than that for silicon (15 eV, e.g. [7]). Thus, though fewer displacements per incident ion should occur, compared with silicon, an amorphous SiC surface would be expected in the dose range used in these experiments (i.e. 10^{17} to 10^{18} ion cm^{-2}).

2. The high concentration of implanted "foreign" atoms often causes the layer to be in a chemically metastable state [11].

3. The volume change associated with (1) and the extra material introduced by implantation produce a stressed surface layer. The stress state is usually that of biaxial compression in the plane of the surface [12]. Such stresses may be large ($\sim$ 1 GPa) at high doses, although localized in the thin implantation-affected layer. The stresses have been measured by cantilever beam techniques [12], X-ray methods [13, 14] and changes in radial cracking behaviour (e.g. [15]). In this study, these stresses were found to affect fracture behaviour (Sections 4.2, 4.3, 4.4).

4. At high doses, the effects of sputtering (material ejection from the surface) may be significant. The surface analysis results for SiC specimens (Section 3.3) indicate that material lost by sputtering approached that gained by implantation at doses greater than $\sim 10^{18}$ cm^{-2} [16].

3. Experimental details

3.1. Materials

The materials used were of two types: (a) single crystal silicon carbide ((0 0 0 1) orientation) hereinafter referred to as "SiC"; (b) reaction-bonded silicon carbide ("REFEL"). The single crystals were broken from polycrystalline aggregates prepared by the Acheson process, supplied by Arendal Smeltewerk (Norway). They were then cut into thin ($\sim$ 350 μm) slices, parallel to the large (0 0 0 1) basal facet, using a high-speed diamond saw (Capco Q35); specimen alignment was by eye. The polytype(s) of the crystals were not directly determined but, from previous experience with this batch of crystals [17] and the TEM results detailed in Section 4.5, they were certainly hexagonal and probably 6H. The reaction-bonded material was similarly cut from rod supplied by UKAEA Springfields. The preparation route for this type of material has been described by Popper [18], and the resultant microstructure has been described by Sawyer and Page [19]. Typically this consists of $\sim$ 10 μm sized impure silicon carbide grit particles, bonded by the new SiC formed during the reaction-bonding process, with 5 to 10% residual silicon. The new SiC generally takes the form of a substantial epitaxial coating around each original grit particle. Both types of material were lapped and polished using a succession of diamond pastes on laps and cloths, finishing with $\frac{1}{4}$ μm paste.

3.2. Implantation

Specimens were implanted with nitrogen and boron ions at UKAEA Harwell. Nitrogen implantations were performed using the "Pimento" prototype commercial implanter, operating at 80 kV. The beam was estimated to consist of $\sim$ 80% N_2^+ ions [20], which are assumed to dissociate into monatomic nitrogen at 40 kV on impact with the sample; thus the total dose of N is 1.8 times the stated dose of N_2^+. The average dose rate was 5.7 $\mu A\,cm^{-2}$ (3×10^{12} ion cm^{-2}), giving an estimated specimen temperature of 300° C. The specimens were rotated in the beam to ensure dose uniformity. A series of specimens of each material was prepared, the lowest dose being 10^{17} $N_2^+\,cm^{-2}$ and the highest 1.6×10^{18} $N_2^+\,cm^{-2}$. Boron implantations were performed using the Harwell–Lintott isotope separator, operating at 40 kV so that each boron atom would have the same energy as the majority of the nitrogen atoms from the Pimento implanter. Doses and dose rates used were equivalent to those used for the nitrogen implantations (i.e. 10^{17} N_2^+ (80 kV) taken to be approximately equivalent to 2×10^{17} B^+ (40 kV)). Specimens were used in the as-implanted, unannealed state. If it is assumed that the stopping rate of ions in SiC is similar to that for silicon, a mean ion range of ~ 0.2 μm would be expected, with a standard deviation of ~ 0.7 μm [7].

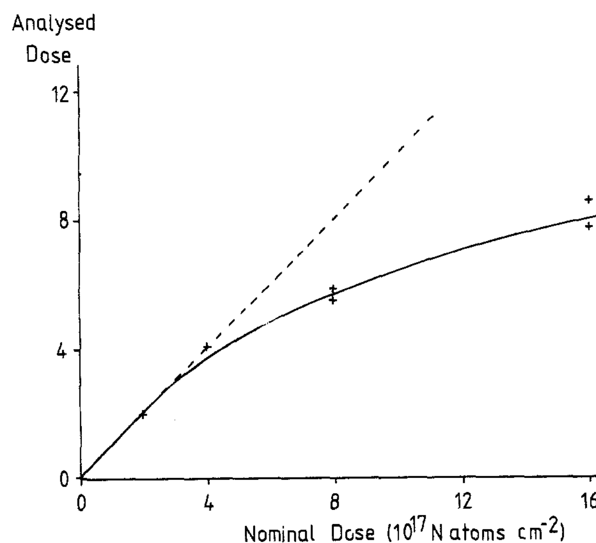

Figure 1 Comparison of estimated and analysed doses for nitrogen implantation into REFEL. The analysed doses are lower than those estimated from the beam flux and implantation times at high doses, probably because of surface sputtering.

3.3. Analysis

Analysis of representative specimens was performed by a nuclear reaction method (using the $^{14}N(d, \alpha)^{12}C$ reaction in the Harwell 6 MeV van de Graaff accelerator). Results showed that, while the doses estimated from the dose rate and implantation times were accurate at low doses, there was a steady divergence between the two at higher doses ($> \sim 4 \times 10^{17} N_2^+ cm^{-2}$) (see Fig. 1). This is presumably due to surface sputtering which removes implanted material from the specimen. Signs of sputtering (pitting, etching) could be seen in the most heavily dosed specimens (e.g. see Fig. 9b). Since the doses estimated from ion fluxes are more relevant to specimen preparation, and as analysis was not performed on all specimens because of time constraints on the van de Graaff facility, it is these estimated doses, rather than sputter-corrected or as-analysed values, that are referred to throughout this paper.

3.4. Microhardness testing and analysis

Specimens were indented using a Leitz "Miniload" machine, fitted with a Vickers profile indenter. Tests were performed at room temperature in air, using a dwell time of 15 sec. The load range used was from 50 to 100 g. Indentations ranged in size from 5 to 30 μm diagonal, and therefore $\sim \frac{3}{4}$ to $\sim 4\,\mu$m depth. Thus the minimum indentation depth is much greater than the thickness of the implanted layer ($\sim 0.3\,\mu$m) and the depth of the "plastic zone" associated with the indentation would be expected to be larger still [21]. However, the simple microhardness testing equipment used here cannot be used to produce reliable indentations much smaller than a few micrometres diagonal. Other workers [22, 23] have used specialized ultra-low-load microhardness equipment to investigate the properties of ion-implanted surfaces. In this case, however, analysis of the indentation size effect (ISE) [24] was used to give a semi-quantitative evaluation of the flow behaviour of the implanted layer.

The indentation size effect (ISE) is the progressive variation in measured hardness with indentation size; the effect is usually most noticeable at loads below ~ 200 g. The direction and magnitude of the ISE is characteristic of a particular material in a particular microstructural state [24], and may be characterized by a simple expression originally proposed by Meyer for ball indentations:

$$L = ad^m$$

where L is the applied load, d the indentation diagonal, a a constant, and m the ISE index. This equation is purely empirical, with no mechanistic or physical implications; nonetheless, the behaviour of most materials is found to fit the equation reasonably well down to loads of ~ 1 g. An ISE index of 2 therefore implies that the hardness is constant with changing indentation size. Normally the effect is such that hardness is found to increase with decreasing indentation size (i.e. indenter load), and so most materials have ISE indices less than 2 e.g. [24].

The raw data from the microhardness tests were analysed by a computer program [24], which derived the ISE index (m), and also the hardness value at a standard indentation size of 10 μm ($H_{10\mu m}$). Using these two parameters, the hardness behaviour of variously implanted surfaces can be investigated. The $H_{10\mu m}$ hardness value is useful since it allows hardness values at constant indentation depths to be obtained and compared. This is particularly useful in cases such as those here, where a layered structure is being indented. Although use of a standard indentation of a size less than 10 μm might give more direct information about the implanted layer, calculation of hardness values from indentations of much smaller sizes would require extrapolation of the raw data well outside statistically acceptable limits*. In addition, measuring hardness impressions less than $\sim 10\,\mu$m in diagonal is prone to considerable error.

4. Results

4.1. Microhardness tests

Fig. 2 shows the results of the ISE analysis of microhardness data from tests on (a) nitrogen-implanted REFEL, (b) nitrogen-implanted silicon carbide, and (c) boron-implanted silicon carbide. Each figure consists of graphs of (i) ISE index and (ii) 10 μm hardness against implanted dose. The high load (large diagonal) hardness values were found not to change significantly with dose of either nitrogen or boron. It can be seen that:

1. the behaviour of nitrogen-implanted silicon carbide and of REFEL is essentially the same. A surface softening occurs at doses $> \sim 4 \times 10^{17} N_2^+ cm^{-2}$, indicated by lower values of 10 μm hardness and an increase in the ISE index to a value greater than 2;
2. implantation of boron to the maximum dose used (which approached the sputtering-limited maximum) has no measurable effect on the microhardness behaviour of silicon carbide.

Examination of the indentations in nitrogen-implanted single crystal SiC shows a change in their appearance around the "critical dose" of $\sim 4 \times 10^{17} N_2^+ cm^{-2}$ (see the stereo pairs in Fig. 3). Below this dose, the edges of high-load indentations are surrounded by cracks of the type $\{1\bar{1}01\}$, with occasional lateral cracks breaking out into the surface (see below). Above the 'critical dose", a thin surface layer can be seen to be rumpled at the edge of the indentation, sometimes breaking away from the substrate. This layer seems to have a thickness of $\sim \frac{1}{2}\,\mu$m, i.e. close to the implanted layer thickness.

Thus, it seems that the change in the microhardness behaviour in nitrogen-implanted SiC is due to the presence of a thin, highly plastic layer produced by the implantation, similar to that reported for silicon and alumina [6, 25]. Calculations based on a crude "mean

*Later work using a Knoop profile indenter (depth-to-length ratio $\sim 1:30$) to sample material closer to the surface has shown similar behaviour in a variety of materials [25].

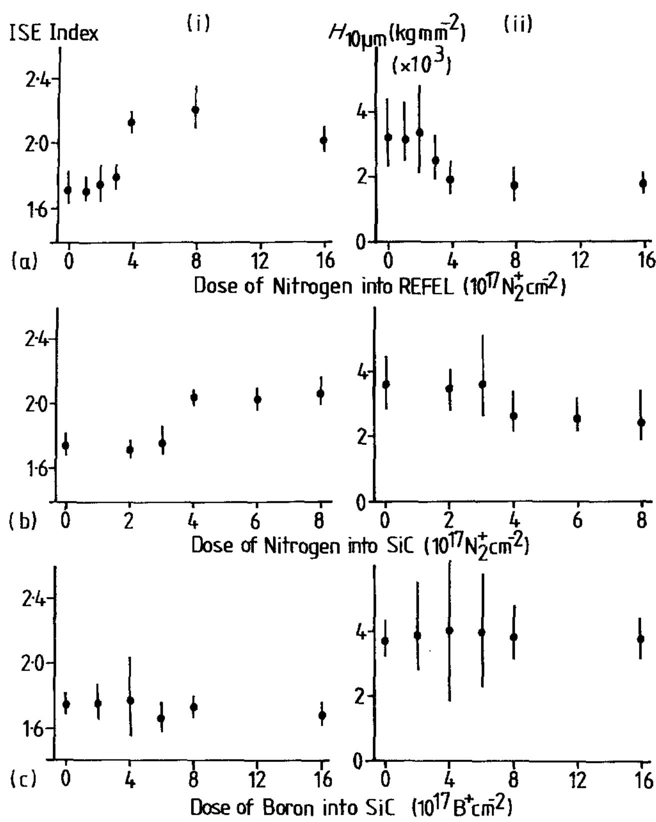

Figure 2 Effects of implantation on the microhardness behaviour of (a) nitrogen-implanted REFEL, (b) nitrogen-implanted single-crystal SiC, (c) boron-implanted single-crystal SiC. Each figure shows both the ISE index and the hardness normalized to a 10 μm indentation size. Note that both surface softening and an increase in the ISE index are induced above $4 \times 10^{17} N_2^+ cm^{-2}$ for nitrogen implantation, and that boron implantation does not significantly alter microhardness behaviour.

hardness", weighted by the volumes of plastically deformed material beneath the indentation lying in the bulk or the implanted layer, indicate that the hardness of the layer is less than $\sim 1000\,kg\,mm^{-2}$, compared to the 'bulk" hardness of $\sim 2700\,kg\,mm^{-2}$. This mean hardness model has been developed by Burnett and Page [6]. Possible microstructural reasons for the change are discussed in the light of the TEM results presented in Section 4.5.

4.2. Indentation fracture of nitrogen-implanted specimens

Nitrogen implantation to high doses was found to have pronounced effects on the fracture behaviour of

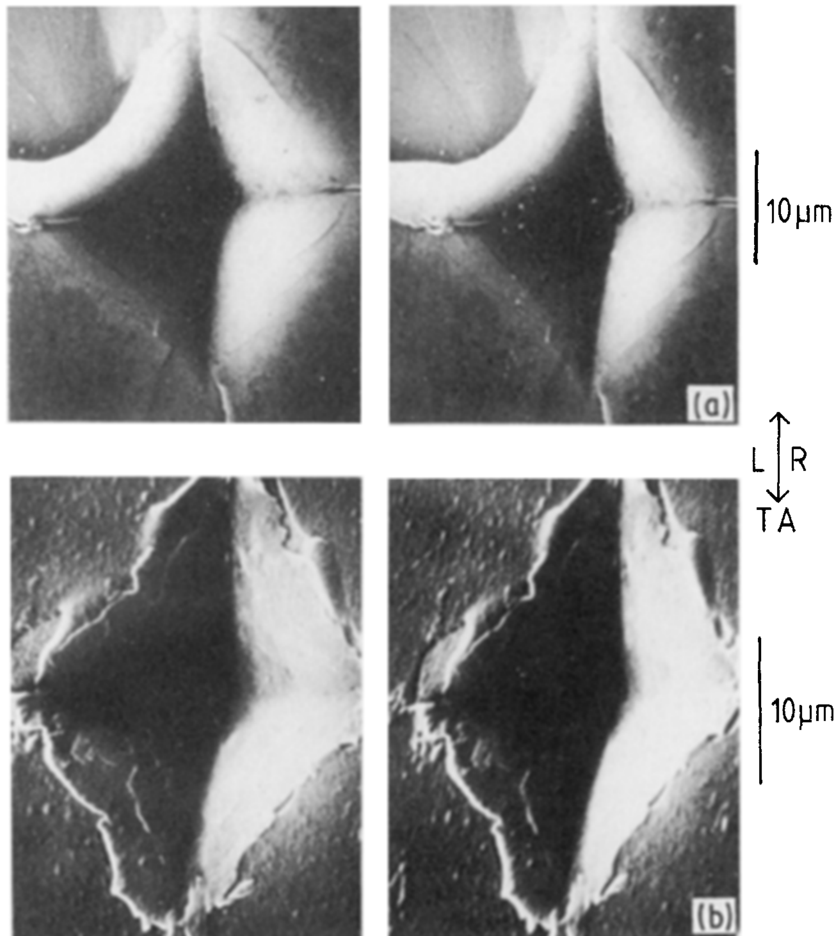

Figure 3 SEM stereopairs (30° (L) and 40° (R) tilts about the tilt axis (TA)) of 1 kg indentations in SiC: (a) dose $6 \times 10^{17} N_2^+ cm^{-2}$; (b) unimplanted. Note the pile-up in (a) and the circumferential and lateral cracking in (b).

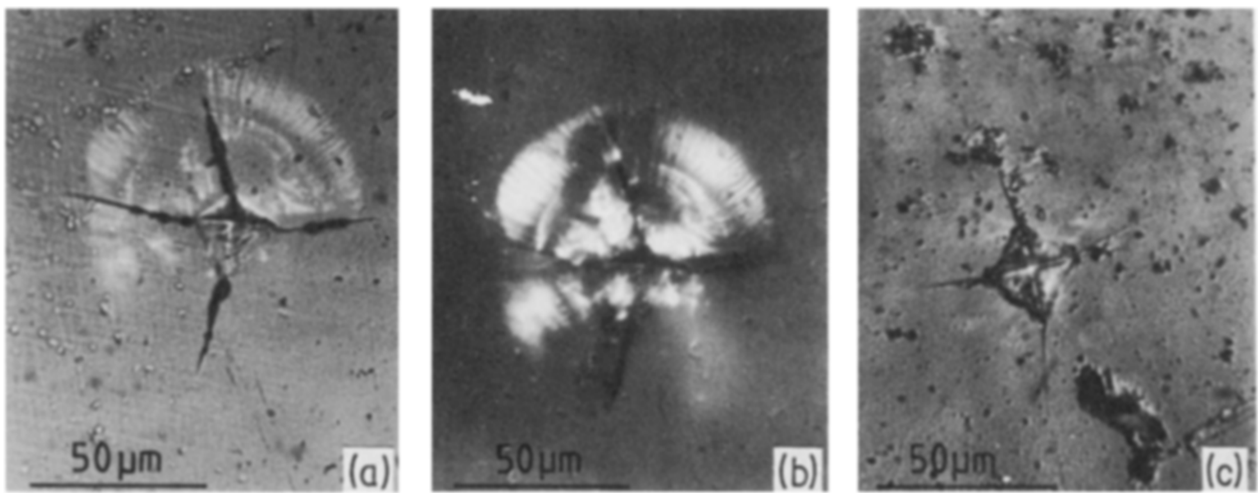

Figure 4 Optical micrographs of 1 kg indentations in single crystal SiC: (a), (b) unimplanted; (c) implanted to $6 \times 10^{17}\,N_2^+\,cm^{-2}$. Note the sub-surface lateral crack "halo" around the indentation in (a), seen better using polarized reflected light in (b). Such effects are not seen in the implanted specimen (c).

silicon carbide (among other brittle materials [4]). The different kinds of fracture around indentations have been described, for example, by Lawn and Wilshaw [26]. Broadly, cracks can be divided into two categories: (a) those where the cracks are normal to the indented surface ("median" and "radial" cracks); (b) those where the cracks are approximately parallel to the indented surface ("lateral" cracks). Lateral cracks in particular result from the action of the residual tensile stress field left after unloading the indenter. Both types of crack can be deleterious to the material's properties; the radial/median cracks can act as flaws for through-thickness fracture, while the lateral cracks can lead to the formation of chips. The effects of implantation in the two SiC materials were similar; the incidence of "broken-out" lateral fracture was suppressed by implantation, while median/radial fracture was not noticeably affected (see Figs. 3, 4 and 5). In the unimplanted state, both materials showed lateral fracture at loads greater than ~ 100 g. The single crystal material ("SiC") showed less tendency than the REFEL to form lateral cracks around indentations.

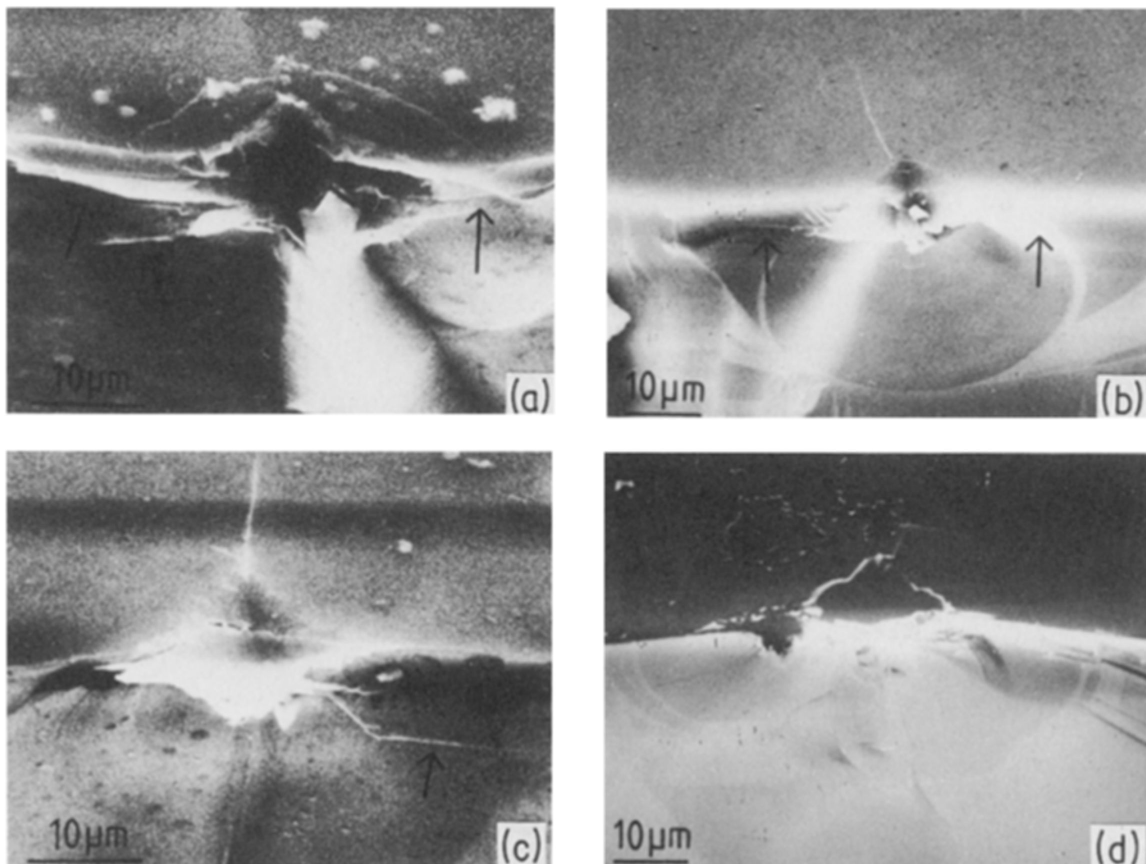

Figure 5 SEM images of 500 g indentations in single crystal SiC, broken open to reveal sub-surface fracture paths: (a), (b) unimplanted; (c) implanted to $4 \times 10^{17}\,N_2^+\,cm^{-2}$; (d) implanted to $6 \times 10^{17}\,N_2^+\,cm^{-2}$. Note increasing suppression of lateral fracture (arrowed) with increasing dose of nitrogen. The shapes of the median/radial cracks can also be seen, as can circumferential cracking in (a) and (b), and pile-up in (d).

This is probably due to the alignment of easy (0 0 0 1) fracture planes parallel to the surface, thus requiring stepping from one such plane to another for breakout to occur (but see results from the boron-implanted specimens (Section 4.3)). In REFEL, the random alignment of fracture planes (both intergranular and intragranular) with the surface increases the likelihood of an easy fracture path being available for breakout.

In general, it was found that visible lateral fracture became increasingly suppressed as the dose increased from 10^{17} to $\sim 10^{18}\,N_2^+\,cm^{-2}$. At the highest doses, no such fracture could be seen. However, observation of the surface alone cannot distinguish easily between the cases of cracks being totally absent and cracks being present but failing to break out. Thus, a variety of techniques were used to explore the incidence of lateral fracture.

Observation of unimplanted SiC by normal incidence reflected light microscopy showed sub-surface lateral fracture as a "halo" surrounding ~ 200 g to 1 kg indentations. The halo was split into four segments by the median/radial cracks; occasionally one segment of the halo was missing. Observation through crossed polars rendered the haloes more visible. These haloes were not visible in heavily implanted samples. This may, however, be due to an implantation-induced change in the optical properties of the near-surface layer rather than to a change in the sub-surface lateral fracture behaviour. It was observed that all implanted specimens had a higher reflectivity than unimplanted ones. These effects are illustrated in Fig. 4.

Observation by the Nomarski differential interference contrast technique revealed the presence of sub-surface fracture by changes in surface tilts. This technique showed the suppression of such fracture in REFEL with increasing dose.

Subsurface lateral fracture in SiC was also investigated by the technique of "breaking open" indentations, whereby indentations were made aligned along a cleavage direction so that the radial/median cracks nearly connected, and were then broken along this line of cracks by three-point bending over the edges of microscope slides. Results from the examination of such specimens in the SEM are shown in Fig. 5. Specimens used were of doses of zero, 4 and $6 \times 10^{17}\,N_2^+$. It was found that:

1. There was a progressive change in lateral crack type and occurrence as dose increased. In unimplanted specimens, lateral fracture was easily observed on both sides of the indentation, often at several levels, and occasionally broken out on to the surface. In the $4 \times 10^{17}\,N_2^+\,cm^{-2}$ specimen, there was usually at least one lateral crack visible; however, these normally propagated well below the surface, some actually being directed away from it. In the $6 \times 10^{17}\,N_2^+\,cm^{-2}$ specimen, very little lateral fracture could be seen at all. The observable cracks were all short and closely associated with the highly disturbed zone immediately beneath the indentation, and breakout did not occur.

2. Samples of all doses showed the "classic" median/radial fracture patterns to some extent. However, some indentations showed an obvious central penny-shaped crack, while in others there appeared to have been separate crack nucleations on either side of the indenter. Both types showed distinguishable extensions to the surface, probably occurring both on unloading the indenter and during the breaking open of the specimen.

3. A highly disturbed region could be seen immediately under all indentations. No change in character of this region with dose was observable; however, details of the region's characteristics were not easily discernible. The localized linear features might be the remnants of fracture, localized shear [27] or phase transformations, etc., and their appearance is probably altered to some extent by the breaking open of the specimen.

Specimens of both materials implanted to doses greater than the critical dose for changes in microhardness behaviour ($\sim 4 \times 10^{17}\,N_2^+\,cm^{-2}$) showed evidence of pile-up around indentations.

SEM examination of the surface around high load (500 g, 1 kg) indentations in SiC often showed a type of fracture approximately parallel to the indentation edge and normal to the surface (see Fig. 3a). The cracks lie along crystallographic directions, the surface intersections being parallel to $\langle 1\,1\,\bar{2}\,0\rangle$. The crack planes are therefore of the form $\{1\,\bar{1}\,0\,l\}$, probably $\{1\,\bar{1}\,0\,0\}$. These cracks are only observed around indentations in zero and low dose specimens. At higher doses the pile-up and exfoliation previously described occurs.

4.3. Indentation fracture of boron-implanted specimens

Indentation fracture was also studied around indentations in the boron-implanted specimens. No lateral breakout was observed in the $16 \times 10^{17}\,B^+\,cm^{-2}$ dose specimens, and only a little around indentations on the $8 \times 10^{17}\,B^+\,cm^{-2}$ dose specimens.

SEM examination of the high dose specimens showed no pile-up or thin-layer "extrusion" of the type noted in the nitrogen-implanted samples. The cracking near to and parallel to the indentation edges appeared somewhat, but not totally, suppressed at these high doses. The indentations appeared slightly "pin-cushioned" compared to indentations on unimplanted material (Fig. 6). Signs of sputtering were visible on the sample surfaces of roughly the same severity as those on equivalently dosed N_2^+ samples.

In order to investigate the possible existence of sub-surface lateral cracks in the high dose specimens, a broken-open specimen of 500 g indentations on $16 \times 10^{17}\,B^+\,cm^{-2}$ material was prepared. A typical section is shown in Fig. 6. It appears that the plane of the specimen's surface was cut slightly inclined to the (0 0 0 1) plane, since all lateral fractures visible beneath the surface were tilted at about 10° to it. This was quite useful, since it can be seen that, while the downward arm of the lateral cracks (which were found beneath all indentations) extend to some distance

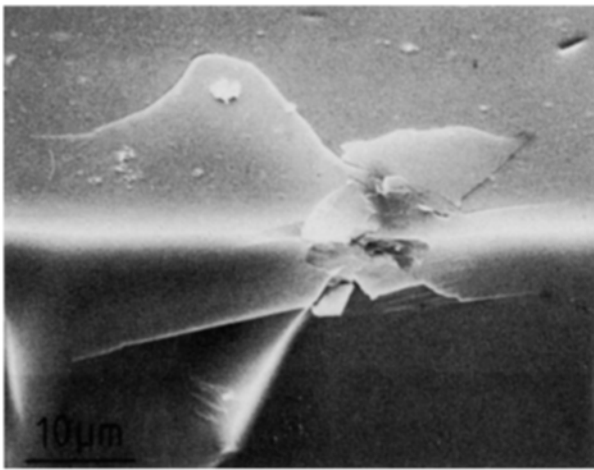

Figure 6 SEM image of broken-open 500 g indentation in boron-implanted SiC ($16 \times 10^{17}\,B^+\,cm^{-2}$). From the orientation of the lateral cracks, the (0 0 0 1) fracture plane appears to be inclined at $\sim 10°$ to the surface. Note the diversion of the upward arm of the crack. The indentation appears slightly "pin-cushioned" when viewed on the original test surface (upper half of figure).

away from the indentations, the upward arms of the cracks stop, or in some cases are diverted, as they approach the surface. This indicates that there is some property of the implanted layer which tends to prevent cracks from approaching it. Since the influence seems to be effective $\sim 3\,\mu m$ beneath the surface, it is likely to be associated with the implantation-induced stress field rather than with the surface microstructure.

4.4. Scratch tracks

Scratch tracks were made by drawing specimens at low speeds ($0.05\,mm\,sec^{-1}$) beneath a loaded diamond cone. 90° diamond cones, and loads of 10, 20 and 50 g were used. The tracks were aligned with the $\langle 1\,1\,\bar{2}\,0\rangle$ directions on the single crystal specimens (i.e. parallel to the $\{1\,\bar{1}\,0\,0\}$ growth facets). Because of play in the bearings of the scratching equipment, alignment inaccuracies were probably up to $\sim 5°$. For most of the scratching experiments only six fresh, sharp cones were available. Consequently, to ensure consistency of results, the usage of each cone was recorded and the tip sharpness frequently examined. After each short series of tests on implanted material, a track was made on unimplanted material, so that the effect of cone blunting on track morphology could be distinguished from the effects of implantation. Consistent differences between the behaviour of implanted and unimplanted SiC were seen (see below) once the initial extreme sharpness of the cones had worn off; this occurred after the cones had made about 0.5 mm of track on SiC, during which samples of all doses showed large amounts of chipping fracture.

Tracks were examined by light microscopy and SEM. Debris was removed from the tracks using Bioden RFA replicating plastic film. Some scratched specimens were "back-thinned" and examined in the TEM; results from such specimens are reported in Section 4.5.

Scratch tracks on nitrogen-implanted single crystal SiC were made on specimens covering the dose range

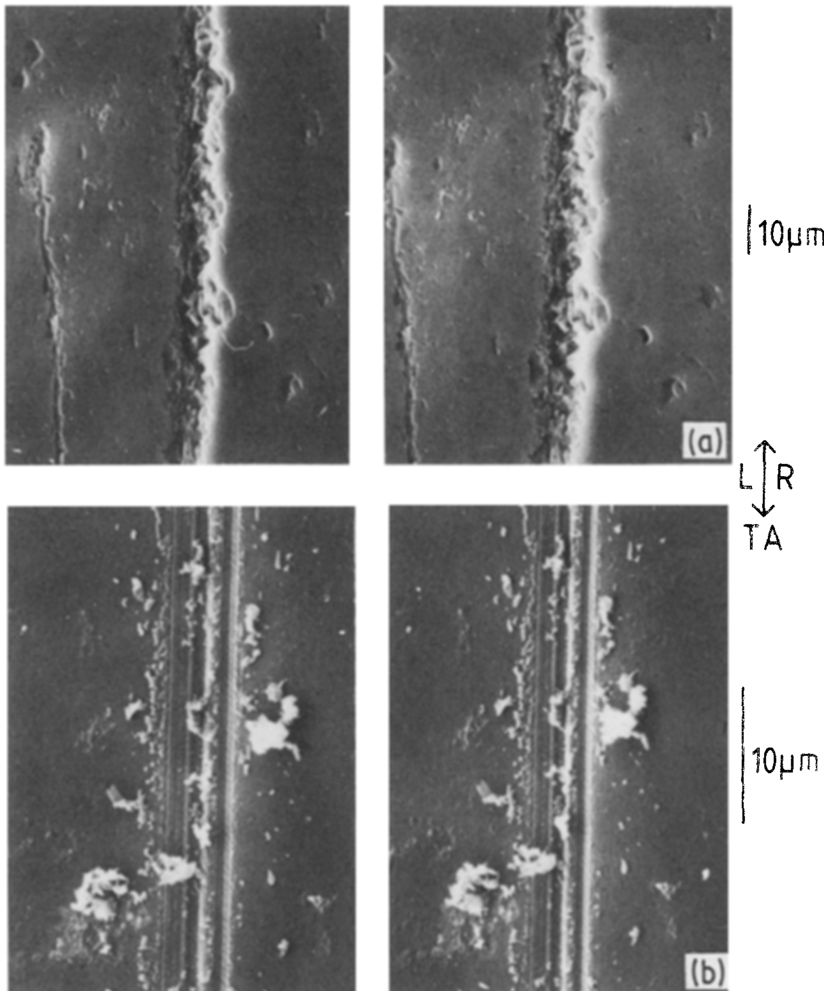

Figure 7 SEM stereopairs (30° (L) and 40° (R) tilts) of scratch tracks in SiC: (a) unimplanted, 10 g load; (b) dose $6 \times 10^{17}\,N_2^+\,cm^{-2}$, 20 g load. Chipping is evident in (a), but in (b) the track appears as a plastically formed groove.

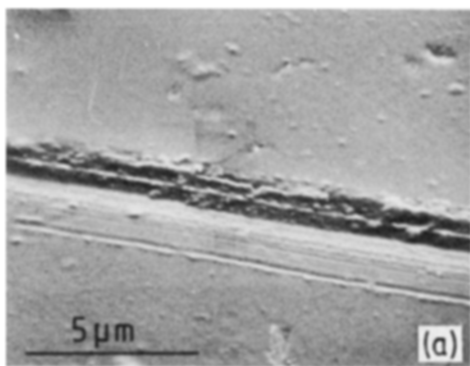

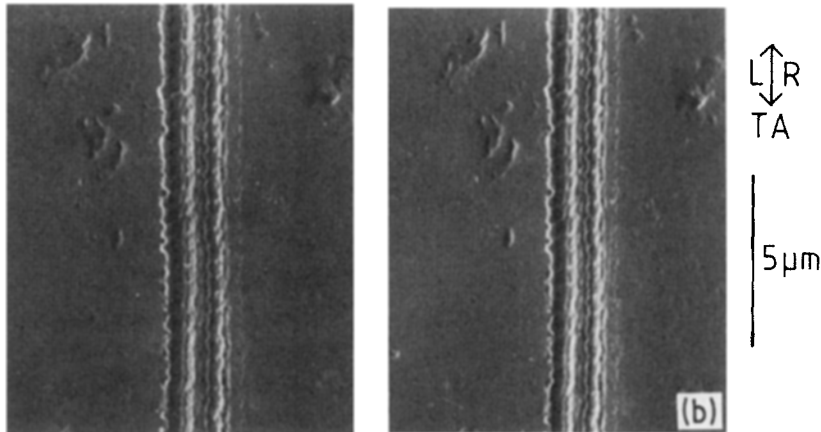

Figure 8 SEM images of scratch tracks in boron-implanted SiC: (a) dose $8 \times 10^{17}\,B^+\,cm^{-2}$, 50 g load. (b) Stereopair (30° and 40° tilts), dose $2 \times 10^{17}\,B^{-2}$, 10 g load. Note the absence of chipping (compare to Fig. 7a).

0 to $6 \times 10^{17}\,N_2^+\,cm^{-2}$. Lateral fracture (chipping) was found to be suppressed in all the implanted samples (minimum dose $2 \times 10^{17}\,N_2^+\,cm^{-2}$) at all loads used (10 to 100 g). Even with a very blunt cone, loads as low at 10 g produced extensive chipping on unimplanted samples. With chipping suppressed by implantation, the groove left by the cone was essentially fully plastic in nature. This is shown in Fig. 7. The track widths appear to be the same (5 to 7 μm for 10 g loads) for both implanted and unimplanted samples, but it is difficult to measure the track widths on the highly fractured unimplanted samples accurately.

Scratch tracks were also made on boron-implanted specimens of SiC. On all the implanted specimens, all tracks appeared as purely plastic grooves; virtually no chipping was seen at any load or dose. The zero-dose reference sample showed chipped tracks at all stages of the tests. Typical results are shown in Fig. 8. These results imply that the softening of the surface for the N_2^+ implanted samples is not primarily responsible for the suppression of chipping fracture, which also occurs in the unsoftened B-implanted samples.

Because of the limited number of cones available, only a small number of tracks were made on REFEL. Specimens used were of doses of zero, 1 and $8 \times 10^{17}\,N_2^+\,cm^{-2}$. As with the single crystal material, the unimplanted sample was used as a reference for checking the effects of cone blunting. Tracks on the low dose specimen showed almost no chipping, even at high loads and with relatively sharp diamonds. For the high dose specimen, chipping was similarly absent. Tracks on the unimplanted material showed large amounts of chipping, even at low loads and with blunt diamonds. Typical tracks are shown in Fig. 9. Measurement of track widths showed the zero and low dose specimens to have track widths of $\sim 3\,\mu$m at 10 g load, as opposed to $\sim 6\,\mu$m on the high dose specimen. Since both the implanted specimens behaved similarly as regards near-track fracture, this indicates that the softening caused by implantation is not very significant in altering the fracture behaviour of the material.

4.5. TEM examination of implanted SiC

Initially, plan view specimens of implanted and unimplanted SiC were prepared by ion-beam machining from the unimplanted side only (i.e. "back-thinned"). Within the usable thickness of the material, all implanted specimens were found to be microcrystalline, producing diffraction patterns consisting of well-defined rings (see Fig. 10a)†. Dark-field images taken from any of the rings illuminated discrete microcrystals of ~ 100 nm diameter (Fig. 10b). No differences were found between the diffraction patterns of specimens implanted to doses above and below the "critical dose" of $\sim 4 \times 10^{17}\,N_2^+\,cm^{-2}$.

In order to investigate further the possible differences between implanted and unimplanted SiC samples, in particular in their response to deformation, similar plan-view specimens were prepared from material scratched as described in Section 4.4. A blunt diamond was used, at a load of 10 g. The thinning of the specimens was stopped when the hole thus produced intercepted the base of the scratch tracks.

†In contrast to these observations, both McHargue and Williams [34] and Burnett [35] have observed, using Rutherford back-scattering techniques, that amorphization occurs in SiC implanted to high doses.

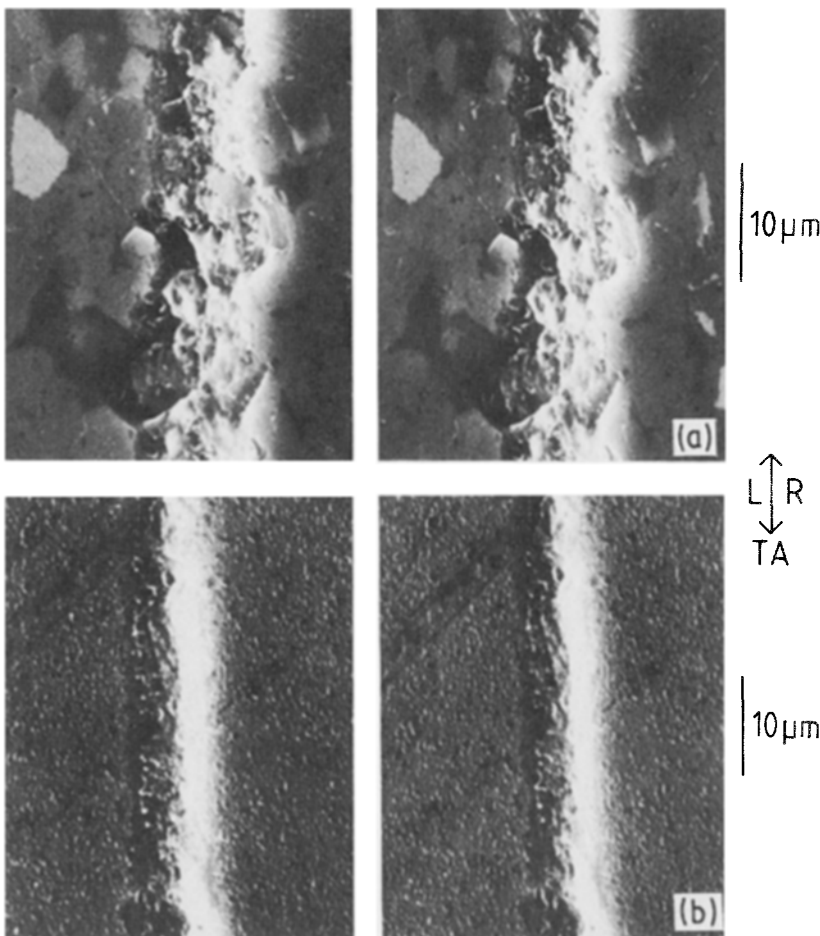

Figure 9 SEM stereopairs (30° and 40° tilts) of scratch tracks (10 g loads) in REFEL: (a) unimplanted; (b) implanted to $8 \times 10^{17} N_2^+ cm^{-2}$. The chipping evident in (a) is totally suppressed in (b). In (b) note also the surface roughening by sputtering.

Specimens were successfully prepared only of zero and $8 \times 10^{17} N_2^+ cm^{-2}$ dose specimens. Selected-area diffraction patterns from these specimens are illustrated in Fig. 10c and 10d (unimplanted) and 10e and 10f ($8 \times 10^{17} N_2^+ cm^{-2}$). For the zero dose specimen it was seen that:

1. both the sub-track and normal material gave diffraction patterns characteristic of hexagonal (α) SiC

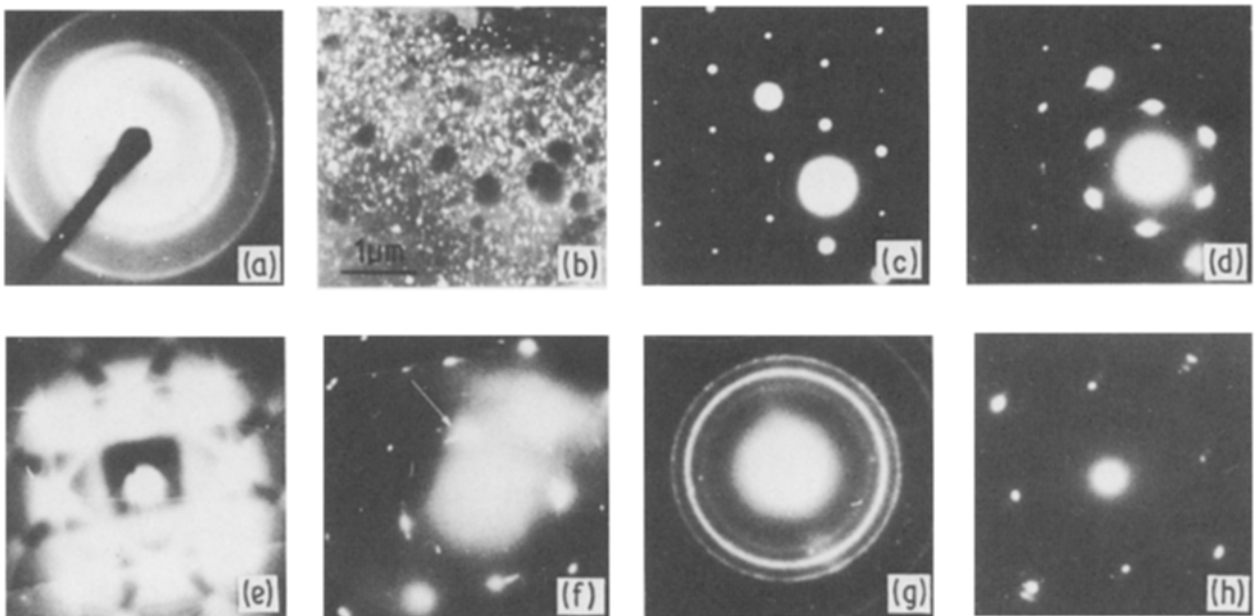

Figure 10 Transmision electron diffraction patterns and micrograph of deformed and/or implanted SiC: (a) Selected-area diffraction pattern (SADP) from an undeformed specimen of dose $3 \times 10^{17} N_2^+ cm^{-2}$. (b) Centred dark-field image of an underformed specimen of dose $6 \times 10^{17} N_2^+ cm^{-2}$, using part of the outer diffracted ring of SADP as in (a); note microcrystalline structure. (c) SADP from unimplanted, undeformed SiC. (d) SADP from unimplanted SiC, deformed by scratching with 10 g loaded diamond cone. Note spot smearing and streaking produced by deformation; however, the material is still hexagonal. (e), (f) SADPs ((e) with Kikuchi lines) of SiC, dose $8 \times 10^{17} N_2^+ cm^{-2}$, scratched (10 g load). SADPs correspond to $\{1\,0\,0\}$ cubic, with some spot streaking (e.g. arrowed in (f)). (g) SADP from undeformed SiC, boron-implanted to $16 \times 10^{17} B^+ cm^{-2}$; note rings characteristic of microcrystalline structure (but different from (a)). (h) SADP from SiC, boron-implanted to $16 \times 10^{17} B^+ cm^{-2}$, scratched (10 g load). SADP corresponds to $\{1\,0\,0\}$ cubic.

(Fig. 10c);

2. diffraction patterns taken from material close to the track showed spot smearing, due to the high degree of deformation in this region (Fig. 10d);

3. the details of the deformation mechanism beneath the track were not resolvable. The region appeared highly disturbed.

For the high dose specimen (see Figs. 10e and f), somewhat different results were found, in particular:

4. diffraction patterns produced from the sub-track area (the only area on this specimen thin enough to transmit electrons) were consistently characteristic of cubic material (β-SiC) (Figs. 10e and f);

5. spot streaking and rotation, similar to that described in (3) above, can be seen. Use of different "subspots" to form dark-field images showed small regions of slightly differing orientation;

6. the cubic material observed was all close to a single orientation, however, as no diffraction patterns could be obtained from the non-scratched part of the specimen, the exact orientation relationship between the new cubic phase and the old hexagonal one could not be determined.

It was initially thought that the phase-change was due to the β-stabilizing effect of the implanted nitrogen [5, 28], so that heavy deformation of nitrogen-doped non-crystalline SiC might tend to produce this phase rather than α-SiC. It was also thought that the phase change might act to relieve stress and so account for the softening observed in the microhardness tests of N_2^+-implanted material. To investigate these possibilities, a sample of boron-implanted and scratched SiC was prepared (dose $16 \times 10^{17}\,B^+\,cm^{-2}$). Since boron-implanted SiC shows no change in its microhardness behaviour with dose, it was expected that the microstructure near the scratch would be similar to that of unimplanted SiC. However, the transformation to the cubic form was also observed in this specimen (see Figs. 10g and h).

It therefore appears that the supposed α/β stabilizing effects of boron (α) and nitrogen (β) have less effect on the final crystalline form produced by deformation of metastable non-crystalline SiC than simply the low temperature stability of β-SiC compared to α-SiC. The phase change alone does not have any effect on microhardness behaviour, since boron and nitrogen-implanted SiC behave differently in this respect. Although the microstructures of the as-implanted materials were not resolved in these observations, the similarity of the masses of boron and nitrogen, and the equivalence of the implantation conditions used, would imply that the physical effects of implantation on the surface should be nearly identical. However, examination of the ring diffraction patterns from the two specimens shows that the structures are not identical. Measurement of the patterns gives the (approximate) interplanar spacings corresponding to the various rings: nitrogen-implanted: 0.308, 0.245, 0.173, 0.140, 0.122, 0.108, 0.099 nm; boron-implanted; 0.253, 0.218, 0.183, 0.129, 0.109, 0.082 nm. Some of these spacings can be identified with various lengths in the SiC unit tetrahedron (0.308, 0.245/0.253, 0.108/0.109, 0.183 nm) and some with the interplanar spacings of the various SiC polytypes (e.g. 0.218 nm may be (0 0 2) in β-SiC). However, since the diffraction lines from many of the polytypes coincide, no definite conclusions can be drawn about the polytype mixes in the differently implanted specimens, except that they appear to differ. The microstructures of the nitrogen-implanted and boron-implanted SiC after deformation appear identical. The only remaining difference between the characteristics of nitrogen and boron in SiC is that boron is a p-dopant and nitrogen an n-dopant in this wide-gap semiconductor (band gap 2 to 3 eV [29]). It is therefore possible that the differences in the microhardness behaviour of boron-implanted and nitrogen-implanted SiC are due to their different characters as electronic dopants. Mechanisms have been proposed (e.g. [30]), by which doping changes the velocity of dislocations in semiconductors. Such effects have been observed both in compression tests [31, 32] and in microhardness testing [33].

5. Summary and discussion of results on implanted SiC

The results presented in the preceeding sections can be summarized as follows.

1. Implantation with nitrogen to above a critical dose of ~ 3 to $4 \times 10^{17}\,N_2^+\,cm^{-2}$ changed the low load, shallow penetration microhardness behavior, in that a softening was observed at low loads. Boron-implantation, up to a dose of $16 \times 10^{17}\,B^+\,cm^{-2}$, did not significantly change the microhardness behaviour.

2. Lateral fracture was suppressed around indentations in high dose samples (both boron- and nitrogen-implanted). In the boron-implanted samples it was only the breakout that was suppressed; in nitrogen-implanted samples the nucleation of the cracks also appeared suppressed at the highest doses.

3. Pile-up and a consequent exfoliation was observed around indentations in high-dose nitrogen-implanted SiC, but was not seen in boron-implanted SiC.

4. The occurrence of the circumferential cracking observed around unimplanted indentations became reduced with increasing dose of boron or nitrogen. In nitrogen-implanted samples the cracking was eliminated, and effect (3) above occurred, above the critical dose. Indentations in high dose specimens (both ion species) showed a small amount of pin-cushioning.

5. Even the lowest doses of boron or nitrogen produced marked changes in the form of diamond cone scratch tracks. Chipping fracture was eliminated under all but the most severe scratching conditions, and the tracks appeared as plastically deformed grooves.

6. TEM examination showed that a transformation to the cubic form (β-SiC) from microcrystalline matrial occurred beneath scratch tracks in SiC implanted with boron or nitrogen. Similarly scratched unimplanted material remained hexagonal, though highly deformed.

From the above it may be deduced that:

(a) the softening observed in nitrogen-implanted

SiC cannot be caused by the observed phase change, nor by any purely physical effects of ion "stuffing";

(b) at first sight, the only simple difference between boron and nitrogen is their opposite semiconductor doping effects; thus, mechanisms such as that due to Hirsch [30] could be the cause of the softening in the nitrogen-implanted SiC. Alternatively, it may be that one of the effects of nitrogen on surface softening is fine-scale gas bubble formation [35];

(c) the surface stress state‡ is the probable cause of the suppression of lateral breakout on implanted SiC. In nitrogen-implanted SiC, the additional reduced nucleation of the cracks is possibly connected with the softening effect of the implantation, perhaps by aiding blunting of crack nuclei. The surface stresses, perhaps by promoting elastic recovery, are also the probable cause of the pin-cushioning of indentations in high-dose specimens;

(d) the changes in scratch track topography in implanted SiC are not primarily connected with surface softening, as the effect is the same for both boron-implanted and nitrogen-implanted material. The suppression of chipping by surface stresses, as for indentation fracture, is the likely controlling effect;

(e) β-SiC (cubic) seems to be the low temperature stable state of SiC, and the presence of supposedly α-stabilizing nitrogen in large amounts does not affect this.

Unexplained observations in this study include the existence (and magnitude) of the critical dose for microhardness effects in nitrogen-implanted SiC. If the softening effect is due to the influence of semiconductor doping on dislocation mobility, then the very high level of nitrogen implanted at the critical dose (a 30 to 50% solution, at peak) would imply that either the proportion of electically active nitrogen is very small, or that the nitrogen has to be present in some quantity at a large depth in the sample to have an effect.

Burnett and Page [6] have attributed the magnitudes of critical doses for softening in silicon implanted with a variety of ion species to the unexpectedly rapid thickening of the amorphous layer with increasing dose. However, the absence of softening for the boron-implanted specimens implies either that additional mechanisms may operate for this ion species in silicon carbide, that the amorphous layer produced by B^+ implantation does not exhibit the same rapid thickening, or that the gaseous nature of the nitrogen implant is significant for the softening observed for this implantation [35].

Our observations of a microcrystalline surface layer in both N_2^+-implanted SiC initially seem at variance with both other observations (e.g. [34, 35]) and predictions (e.g. [6]), in that an amorphous surface would have been expected. Since other workers have observed a truly amorphous surface in SiC implanted to high doses, we cannot discount the possibility that this layer results from the recrystallization of amorphous (or heavily damaged) material during ion-beam thinning for TEM. Furthermore, the production of β-SiC by the low-temperature recrystallization of an amorphized SiC layer resulting from either B-implantation or N-implantation seems more likely than a direct $\alpha \rightarrow \beta$ transformation beneath the scratch tracks. Thus, as expected, amorphized SiC is almost certainly formed by high-dose implantation into SiC.

Acknowledgements

The work reported in this paper was performed as part of an SERC CASE studentship in collaboration with UKAEA Harwell. Implantations were performed with the assistance of Dr G. Dearnaley, Dr D. Chivers and G. Proctor. Laboratory facilities at Cambridge were provided by Professor R. W. K. Honeycombe.

References

1. P. J. BURNETT and T. F. PAGE, *Proc. Brit. Ceram. Soc.* **34** (1984) 65.
2. G. DEARNALEY, *Mater. Eng. Applic.* **1** (1978) 28.
3. S. G. ROBERTS, PhD thesis, University of Cambridge (1983).
4. S. G. ROBERTS and T. F. PAGE, in "Ion Implantation into Metals", Proceedings of the 3rd International Conference on Modification of Surface Properties on Materials by Ion Implantation, UMIST, Manchester, UK June 1981, edited by V. Ashworth, W. S. Grant and R. Procter (Pergamon Press, London, 1982) p. 135.
5. N. W. JEPPS and T. F. PAGE, *J. Cryst. Growth* **7** (1983) 259.
6. P. J. BURNETT and T. F. PAGE, *J. Mater. Sci.* **19** (1984) 845.
7. G. CARTER and W. S. GRANT, "Ion Implantation of Semiconductors" (Edward Arnold, London, 1976).
8. L. A. CHRISTEL, J. F. GIBBONS and T. W. SIGMON, *J. Appl. Phys.* **52** (1981) 7143.
9. I. A. HØNSTVET, R. E. SMALLMAN and P. M. MARQUIS, *Phil. Mag.* **41A** (1980) 201.
10. B. HUDSON and B. E. SHELDON, *J. Micros.* **97** (1973) 113.
11. J. M. POATE and A. G. CULLIS, in "Ion Implantation in Materials Science and Technology", edited by J. K. Hirvonen (Acacemic Press, New York, 1980).
12. E. P. EERNISSE, *J. Appl. Phys.* **45** (1974) 167.
13. O. ALSTRUP, *Phys. Status Solidi* **51A** (1979) 407.
14. R. N. KYUTT, P. V. PETRASHEN and L. M. SOROKIN, *ibid.* **60A** (1980) 381.
15. P. J. BURNETT and T. F. PAGE, *J. Mater. Sci.* **19** (1984) 3524.
16. Z. L. LIAU and J. W. MAYER, *J. Vac. Sci. Technol.* **15** (1978) 1629.
17. G. R. SAWYER, P. M. SARGENT and T. F. PAGE, *J. Mater. Sci.* **15** (1980) 1001.
18. P. POPPER, in "Special Ceramics", edited by P. Popper (Heywood, London, 1960) p. 209.
19. G. R. SAWYER and T. F. PAGE, *J. Mater. Sci.* **13** (1978) 885.
20. G. PROCTOR, private communication (1980).
21. J. LANKFORD and D. L. DAVIDSON, *J. Mater. Sci.* **14** (1979) 1669.
22. J. B. PETHICA, in "Ion Implantation into Metals", Proceedings of the 3rd International Conference on Modification of Surface Properties on Materials by Ion Implication, UMIST, Manchester, UK, June 1981, edited by V. Ashworth, W. S. Grant and R. Procter (Pergamon Press, London, 1982) p. 147.
23. D. NEWEY, H. M. POLLOCK and M. A. WILKINS *ibid.*, p. 157.
24. P. M. SARGENT and T. F. PAGE, *Proc. Brit. Ceram. Soc.* **26** (1978) 209.

‡Since this study, a more detailed study of surface stresses resulting from ion implantation has been undertaken [36].

25. P. J. BURNETT and T. F. PAGE, in "Deformation of Ceramic Materials", edited by R. E. Tressler and R. C. Bradt (Plenum Press, New York, 1984), p. 669.
26. B. R. LAWN and T. R. WILSHAW, *J. Mater. Sci.* **10** (1975) 1049.
27. J. T. HAGAN, *ibid.* **15** (1980) 1417.
28. A. R. KIEFFER, P. ETTMAYER, E. GUGEL and A. SCHMIDT, *Mater. Res. Bull.* **4** (1969) S153.
29. M. C. PARCHE, in "Kirk-Olmer Encyclopaedia of Chemical Technology", Vol. 4 (Wiley, New York, 1964) p. 114.
30. P. B. HIRSCH, in Proceedings of the Symposium on Defects in Semiconductors, Boston, Mass, USA, edited by J. Narayan and T. Y. Tan (Horth-Holland, New York, 1981) p. 257.
31. A. GEORGE and G. CHAMPIER, *Phys. Status Solidi*, **53a** (1979) 529.
32. J. RABIER, P. VEYSIERRE and J. L. DEMENET, *J. Phys. Colloque* **44** (1983), C4-243.
33. S. G. ROBERTS, P. PIROUZ and P. B. HIRSCH, *ibid.* **44** (1983) C4-75.
34. C. J. MCHARGUE and J. M. WILLIAMS, *Proc. Mater. Res. Soc.* **7** (1982) 303.
35. P. J. BURNETT, private communication (1984).
36. P. J. BURNETT and T. F. PAGE, *J. Mater. Sci.* **20** (1985) 4624.

Received 18 February
and accepted 13 March 1985